www.czasopisma.pan.pl PAN www.journals.pan.pl
POLSKA AKADEMIA NAUK

Metrol. Meas. Syst., Vol. 28 (2021) No. 4, pp. 627–642
DOI: 10.24425/mms.2021.137698

PAN POLSKA AKADEMIA NAUK

METROLOGY AND MEASUREMENT SYSTEMS

Index 330930, ISSN 0860-8229
www.metrology.wat.edu.pl

M&MS

METROLOGY AND CONTROL OF ELECTROMAGNETICALLY ACTUATED CANTILEVERS USING OPTICAL BEAM DEFLECTION METHOD

Daniel Kopiec[1], Wojciech Majstrzyk[2], Bartosz Pruchnik[1], Ewelina Gacka[1], Dominik Badura[1], Andrzej Sierakowski[2], Paweł Janus[2], Teodor Gotszalk[1]

1) *Wrocław University of Technology, Faculty of Microsystems Electronics and Photonics, Department of Nanometrology, Janiszewskiego 11/17, Wrocław 50-372, Poland* (*daniel.kopiec@gmail.com, wojciech.majstrzyk@pwr.edu.pl, ewelina.gacka@pwr.edu.p,* ✉ *bartosz.pruchnik@pwr.edu.pl,* +48 713 202 573, *teodor.gotszalk@pwr.edu.pl*)

2) *Łukasiewicz Research Network, Institute of Microelectronics and Fotonics, Lotników 32/46, Warsaw 02-668, Poland* (*andrzej.sierakowski@imif.lukasiewicz.gov.pl, pawel.janus@imif.lukasiewicz.gov.pl*)

Abstract

In this paper, we present metrology and control methods and techniques for electromagnetically actuated microcantilevers. The electromagnetically actuated cantilevers belong to the micro electro mechanical systems (MEMS), which can be used in high resolution force and mass change investigations. In the described experiments, silicon cantilevers with an integrated Lorentz current loop were investigated. The electromagnetically actuated cantilevers were characterized using a modified optical beam deflection (OBD) system, whose architecture was optimized in order to increase its resolution. The sensitivity of the OBD system was calibrated using a reference cantilever, whose spring constant was determined through thermomechanical noise analysis registered interferometrically. The optimized and calibrated OBD system was used to observe the resonance and bidirectional static deflection of the electromagnetically deflected cantilevers. After theoretical analysis and further experiments, it was possible to obtain setup sensitivity equal to 5.28 mV/nm.

Keywords: optical beam deflection, thermomechanical noise, low frequency noise, electromagnetically actuated cantilever, Lorentz force.

© 2021 Polish Academy of Sciences. All rights reserved

1. Introduction

Since the early 80s, technologies used for semiconductor fabrication have been adapted for manufacturing of *microelectromechanical systems* (MEMS) [1]. Recently, this field has grown rapidly including the development of a variety of resonators, pumps, mass change and inertial sensors, optical switches, and many other microdevices [2]. All the necessary components of the modern MEMS devices are manufactured and integrated in one structure using microelectronic technologies. Additionally, the miniaturization of the force sensors implies the increase in the detection resolution and a reduction of the interactions, which can be observed.

Copyright © 2021. The Author(s). This is an open-access article distributed under the terms of the Creative Commons Attribution-NonCommercial-NoDerivatives License (CC BY-NC-ND 4.0 https://creativecommons.org/licenses/by-nc-nd/4.0/), which permits use, distribution, and reproduction in any medium, provided that the article is properly cited, the use is non-commercial, and no modifications or adaptations are made.

Article history: received March 17, 2021; revised June 9, 2021; accepted June 24, 2021; available online July 4, 2021.

Cantilever structures belong to the most universal MEMS force sensors. Their functionality can be complete when a deflection actuator is integrated with the beam mechanical structure. In this way a technique for reliable, repeatable and very efficient actuation of the static and resonance structure displacement is ensured. Application of the described MEMS devices makes it possible to investigate interactions in the range from piconewtons up to micronewtons. In order to investigate the force interactions metrologically technology for determination of MEMS properties and cantilever displacement must be developed.

In MEMS technology there are a few methods which have been used to control the deflection of movable micromechanical parts. electrostatic, piezoelectric, electromagnetic and electrothermal techniques are among the most representative ones [3].

In the electrothermal technique, mechanical stress in the mechanical structure is induced thermally which leads to structure deflection. This method was applied to excite resonance vibration, although the static deflection could be controlled only in one direction [4].

The microfabrication of electromagnetically actuated cantilevers was proposed for the first time by Shen *et al.* [5]. In recent years, electromagnetic cantilevers were applied as high resolution magnetic field sensors [6, 7], resonators [8] and probe cantilevers in atomic force microscopy [9, 10]. In the electromagnetic technology, when a cantilever is immersed in the magnetic field and when electrical current passes through the Lorentz loop, the electrodynamic force makes the structure deflect. Through the control of the drive current it is possible to control not only the direction, but also the frequency of structures displacement.

In order to optically observe the cantilever deflection either interferometric technology or *optical beam deflection* (OBD) methods can be applied [1, 11, 12]. The OBD technology was also applied in bio-chemical sensors applications, in which cantilever bending was an indication of chemical, physical or biological processes occurring on the beam surface [13–16]. In this technique, the position of the beam reflected from the cantilever on a *position sensitive* detector (PSD) is the measure of cantilever deflection. The OBD technique can be implemented in liquid and vacuum systems and provides high sensitivity and detection resolution which is comparable with the interferometric techniques [11, 17–19]. The force and displacement nanometrology using MEMS tools includes also development and application of reliable, well understood, and easy to be applied calibration procedures [20]. It is necessary to notice that a metrological OBD setup requires interaction of many independent physical phenomena. Hence the optimisation process of OBD setup construction needs one common quantity to describe metrological parameters. Disregarding many integrated physical processes, an OBD metrological head needs to be described primarily by sensitivity both theoretically and experimentally.

In this paper, we present a metrological OBD setup (called EmagCan-OBD) for static deflection and vibration measurements of electromagnetically actuated cantilevers (called EmagCan structures). The developed setup is optimized in order to be applied in quantitative and not only qualitative investigations of cantilever deflection. The PSD output signal is normalized by the total signal received by the PSD detector, making the OBD system insensitive to the instabilities of incident beam power. To improve the sensitivity of the deflection measurements a slit aperture and precisely adjusted optical components in the EmagCan-OBD optical path are used. As a calibration standard, an EmagCan-OBD reference structure of defined geometry is applied. Prior to experiments, its thermomechanical noise was analysed interferometrically to determine the reference cantilever stiffness. Application of the EmagCan-OBD reference standard allowed us to compare results of the numerical calculations of measurement sensitivity influenced by the size and shape of the incident laser beam with the results of the experiments performed. The conducted optimization led to the 7-fold reduction of laser *relative intensity noise* (RIN). More-

Metrol. Meas. Syst., Vol. 28 (2021), No. 4, pp. 627–642
DOI: 10.24425/mms.2021.137698

over, the sensitivity of the developed EmagCan-OBD setup increased 3.5-fold. Both experimental assumptions are in good agreement with theoretical calculations.

The optimized EmagCan-OBD setup was used for static measurements of the Lorentz force actuated cantilevers manufactured at the Institute of Microelectronics and Photonics of the Łukasiewicz Research Network [22]. In this paper we show the actuation of the electromagnetically and thermomechanically induced cantilever movements. Moreover, we show how to calculate the actuation sensitivities of both actuation modes, which is of crucial importance for further applications, including nanomanipulation and force metrology.

2. Theory of EmagCan-OBD measurement setup

A typical experimental setup of an OBD detector is presented in Fig. 1a. The diverging beam of the laser diode is collimated by a collimator with focal length f_C, and then the beam is focused on the cantilever by a focusing optics with focal length f_F. The light is reflected from the cantilever directly onto a PSD. The cantilever's displacement Δz is transformed into the laser spot's displacement Δy on the PSD in vertical directions and Δx in a horizontal direction – Fig. 1b. Under the assumption of circular deformation of the cantilever the relation between the displacements takes the form of [23, 24].

$$\Delta z = \frac{l}{4s}\Delta y, \tag{1}$$

where Δz is the vertical displacement of the cantilever apex, Δy is the angular displacement of the laser spot on the PSD, l is the cantilever length, s is the distance between the tip and the PSD.

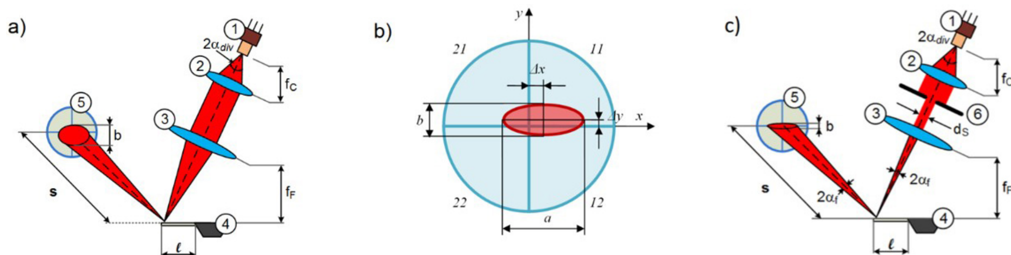

Fig. 1. a) Basic diagram of EmagCan-OBD cantilever deflection setup architecture; b) Laser spot alignment on the PSD, a and b are horizontal and vertical dimensions, while Δx and Δy are horizontal and vertical displacements of the laser spot; c) Optimized setup of EmagCan-OBD; 1 – semiconductor laser, 2 – collimating lens, 3 – focusing lens, 4 – cantilever, 5 – photodetector, 6 – slit aperture; inclusion of aperture renders the angle of the detection beam smaller, and thereby improves sensitivity as described further in the text.

The position of the laser spot on the PSD is determined by measurement of the photocurrents from the corresponding PSD segments. In the presented analysis we assume the rectangular shape of the laser spot and uniform optical power distribution instead of the Gaussian distribution [25]. The output voltage Δu_V of the current to voltage converter (I/V) for the vertical deflection signal is given by:

$$\Delta u_V = \Delta i_V R_{IV} = 2a\eta P R_{IV}\frac{\Delta y}{b}, \tag{2}$$

where a is the laser power attenuation coefficient in the optical path, η is the efficiency of the light-to-current conversion at the photodiodes, P is the output power of the laser diode, R_{IV} is the

resistance of the feedback resistor in the I/V converter and Δi_V is current induced due to vertical displacement (for horizontal displacement the analysis remains unchanged). When the Δu_V is normalized by the total power signal u_p received at the PSD detector the following formula can be obtained:

$$\Delta u_{VN} = G_N \frac{\Delta u_V}{u_p} = 4G_N \frac{1}{l}\frac{2s}{b}\Delta z, \tag{3}$$

where Δu_{VN} is the normalized voltage signal for the vertical axis, G_N is the amplification or scaling factor of the normalization circuit (in our case 10). The analysis of the path geometry and the function makes it possible to write:

$$\frac{2s}{b} = \frac{f_F}{f_c \tan \alpha_{\text{div}}}, \tag{4}$$

where α_{div} is the laser beam divergence angle in the vertical (perpendicular to the junction plane) axis. Based on equations (3) and (4), the formula enabling calculations of the OBD detection sensitivity can be written as:

$$\frac{\Delta u_{VN}}{\Delta z} = 4G_N \frac{1}{l}\frac{f_F}{f_c}\frac{1}{\tan \alpha_{\text{div}}}. \tag{5}$$

In order to maximize the OBD detector sensitivity with given cantilever length, it is necessary to maximize the ratio of focal lengths f_F/f_c and minimize the divergence angle α of the laser beam. However, the divergence angle of the laser beam is determined by the lens diameter and the increasing of the focal length of the focusing lens leads to an increase in the dimensions of the entire setup. The described problem can be solved by using an aperture in the optical path, to narrow the optical beam and decrease the beam divergence angle. The modified setup with the slit aperture is presented in Fig. 1c. The following proportion can be written for the setup geometry (Fig. 1c):

$$\frac{2s}{b} = \frac{2f_F}{d_s}, \tag{6}$$

where d_s is the width of the slit aperture. The (3) shows that for the high output signal the ratio of $2s/b$ should be increased (this is also visible in (6)), which can be achieved by f_F increasing and/or d_s decreasing. Taking into account the decrease in the optical power caused by the aperture, the respective formula for the detection sensitivity in the aperture setup is:

$$\frac{\Delta u_{VN}}{\Delta z} = 8G_N \frac{1}{l}\frac{f_F}{d_s}. \tag{7}$$

In the modified EmagCan-OBD setup, to maximize the sensitivity, for a given length of the cantilever, it is required to maximize the f_F/d_s ratio. It should be noticed, however, that the smaller aperture slits deteriorate the *signal to noise ratio* (SNR) as the incident power deflected on the cantilever is significantly reduced. The sensitivity of an OBD detector as the function of the width of the laser beam and length of the cantilever is plotted in Fig. 2.

The metrological properties of an OBD detector are described not only by the setup sensitivity but its resolution as well. In this case the noise properties of a semiconductor laser and a read-out electronics must be taken into account [21, 23, 26, 27]. In the noise budget the contribution of the photodetector cannot be calculated.

Metrol. Meas. Syst., Vol. 28 (2021), No. 4, pp. 627–642
DOI: 10.24425/mms.2021.137698

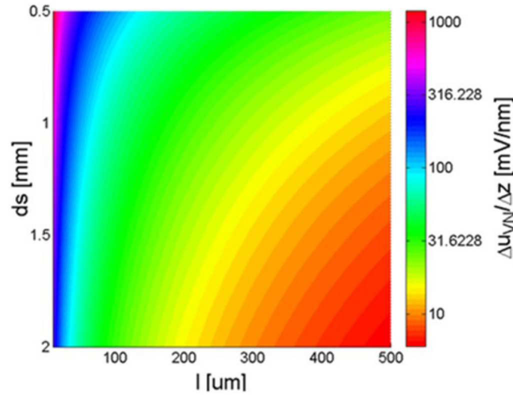

Fig. 2. Numerical analysis of deflection sensitivity $\Delta u_{VN}/\Delta z$ calculated based on (7) as the function of length l of the cantilever and width of the laser beam d_s. The calculations assuming focal length $f_F = 75$ mm and gain factor $G_N = 10$.

The voltage noise density $\frac{\delta u_s}{\sqrt{B}}$ arising from the photodetector thermal noise on the output of the I/V converter of the PSD is given by the equation [21]:

$$\frac{\delta u_s}{\sqrt{B}} = R_{IV}\sqrt{\frac{2e}{a\eta P}}, \tag{8}$$

where B is the considered bandwidth, e is the elementary charge. On the output of the normalization circuit, this noise will be described by the following equation:

$$\frac{\delta u_{sN}}{\sqrt{B}} = \frac{G_N \frac{\delta u_s}{\sqrt{B}}}{u_P} = G_N\sqrt{\frac{2e}{a\eta P}}. \tag{9}$$

Taking this into account, the effective deflection noise density corresponding to the detection threshold is given by the equation:

$$n_{zsN} = \frac{\frac{\delta u_{sN}}{\sqrt{B}}}{\frac{\Delta u_{VN}}{\Delta z}} = \frac{l}{4}\frac{f_c \tan\alpha_{\text{div}}}{f_F}\sqrt{\frac{2e}{\eta a P}}. \tag{10}$$

The effective deflection noise density can be calculated by:

$$n_{zsN} = \frac{l}{4}\frac{\sqrt{f_c d_s \tan\alpha_{\text{div}}}}{f_F}\sqrt{\frac{2e}{\eta a P}}. \tag{11}$$

Taking into account the setup geometry the above equation takes the form of:

$$n_{zsN} = \frac{l}{8}\frac{d_s}{f_F}\sqrt{\frac{2e}{\eta a P}}. \tag{12}$$

Equations (10), (11), (12) show the theoretical limits of noise performance of the designed EmagCan-OBD setup. An analysis of (12) shows that the same rules as for the optimization of the OBD sensitivity apply also to the optimization of setup resolution. Moreover, the measurement resolution increases when the laser operates with higher power. but in this case to find the optimal SNR the noise performance of the laser diode must be analysed as well.

3. Experimental of EmagCan-OBD measurement setup

The designed and fabricated EmagCan-OBD setup is presented in Fig. 3. The source of laser radiation is a semiconductor laser (ThorLabs: L650P007) operating at the wavelength of 650 nm, with 7 mW maximal output power.

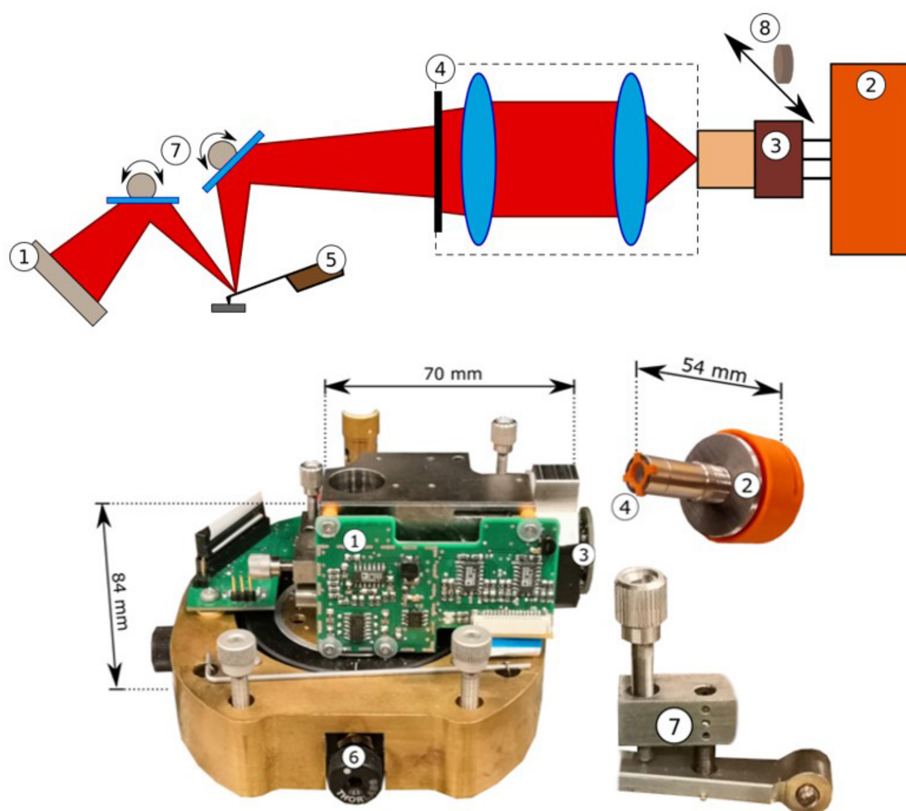

Fig. 3. EmagCan-OBD metrological setup, schematic and photographs with adequate numeration:
1 – precise and low noise PSD I/V converters with a normalization circuit, 2 – semiconductor laser modulator with a RF modulator and an APC controller, 3 – RF modulator and an APC circuit inside the laser housing, 4 – collimation tube with a slit aperture, 5 – socket of an electromagnetically actuated cantilever, 6 – precise XY coarse movement stage, 7 – adjustment mechanism for the PSD mirror positioning, 8 – ball bearing adjustment mechanism for laser adjustment.

In our setup we used a collimator lens of focal length fc 4.5 mm (Thorlabs Collimation Tube with Optic LT 110P-A) and a focusing lens of focal length 50 mm (Thorlabs AC127-050-A). The transimpedance and arithmetic amplifiers were built using AD851x operational

Metrol. Meas. Syst., Vol. 28 (2021), No. 4, pp. 627–642
DOI: 10.24425/mms.2021.137698

amplifiers (Analog Devices). The PSD photodiode (Silicon Sensor: QP50-6-TO8) was reversely biased, providing the bandwidth of 1.5 MHz. Each PSD signal was normalized using an MPY634 analogue multiplier (Texas Instruments). In order to reduce laser intensity noise, low frequency noise and optical feedback coupling, a precise ic-WKN APC laser driver (ic-HAUS) with an RF modulator (Intersil: EL6204) was developed.

The APC driver, operating in the so called slow start regime, is protected against *electrostatic discharge* (ESD) and overheating. It ensures the control of the laser power with the stability of 0.01% over 10 hours. The power spectrum of the thermal noise was recorded using a data acquisition card and the dedicated software. Parameters of microcantilevers were determined by means of measurements conducted using an SP-S 120 series laser interferometric vibrometer (SIOS GmbH). There are several features of the EmagCan-OBD head design, which increase its resolution, reliability and measurement throughput. The optical path was calculated and modelled using CAD software, which led to proper laser beam focusing and its steering. The head was manufactured in the CNC technology, which ensured the required precision of the optical path. The setup was made of stainless steel which increased setup stiffness, and in result, insusceptibility to vibration. In order to reduce the influence of the parasitic light reflections the head inside was blackened and the PSD was embedded in a bushing. All rotating parts were mounted with the use of miniature ball bearings, which made it possible to adjust the laser beam position with high precision and repeatability. In addition, working pairs of precise screws and springs secured the stability of the setup.

4. Results and discussion

In the performed experiments, we observed changes in relative sensitivity of the EmagCan-OBD setup for different optical components of the laser column. Fig. 4 shows the laser spot patterns for varying collimator focal lengths and slit apertures. The laser spots were captured using a 1/1.8″ CCD camera.

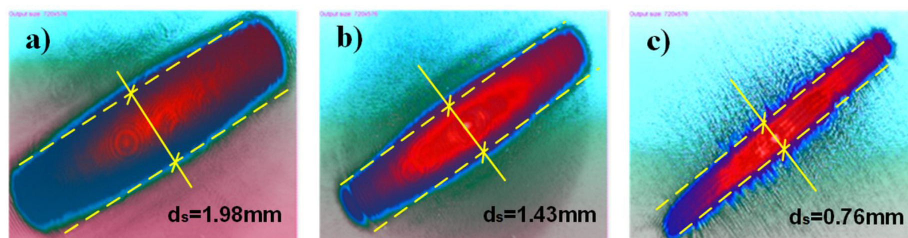

Fig. 4. Image of the laser spot captured with a CCD 1/1.8″ camera with width measurement: a) collimator lens 6.2 mm, width of the laser spot 1.98 mm; b) collimator lens 4.5 mm, width of the laser spot 1.43 mm, c) collimator lens 4.5 mm and a slit aperture, width of the laser spot 0.76 mm.

The power of the laser beam directed on the cantilever was 3 mW for all the applied aperture slits. The obtained results show that the application of the collimator of the shortest focal length made it possible to reduce the spot size to 0.8 mm, which is in agreement with equations (4) and (6). Moreover, in order to ensure the highest measurement resolution the noise properties of the laser were optimized. The qualitative investigations showed, that the RMS noise of the laser radiation could be reduced seven times when RF modulation of the operation current and additional aperture slid were applied, see Fig. 5.

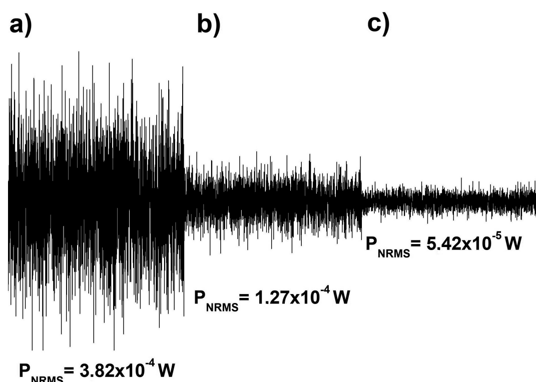

Fig. 5. Laser radiation intensity noise measured by the PSD. The optical power of the beam was 3 mW for every aperture slit The sections in the graph correspond with a) standard laser configuration with APC control, b) laser with APC and RF modulated bias current, c) laser with APC and an RF modulated bias current and a 0.8 mm slit aperture in the optical path.

The quantitative investigations were performed using a setup presented in Fig. 6. As the laser source a system consisting of a Thorlabs L650P007 laser, an APC module based on an ic-WKN (ic-Haus) chip and an EL6204 modulator were applied. The investigated laser beam was directed to a photodetector connected to a differential I/V converter (which made monitoring of the DC laser power also possible). The outputs of the differential I/V converter were connected to a differential voltage amplifier operating in the bandwidth from 0.01 Hz up to 10 kHz. The output of the voltage preamplifier was analysed by a data acquisition card and dedicated software. The differential system architecture made the entire system immune to electromagnetic disturbances.

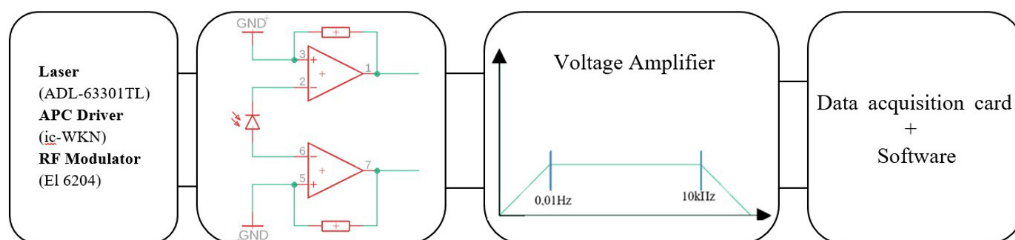

Fig. 6. Block diagram of a measurement setup for characterisation of an EmagCan OBD system.

The results of the low-frequency noise measurements of the EmagCan OBD laser operating at various output power with and without an RF modulator are shown in Fig. 7. In order to analyze the role of the RF bias, current modulation power of the low-frequency noise in the bandwidth was calculated for every power of the EmagCan laser, and the results are summarized in Table 1. It can be seen that the noise to power (PN/P) ratio increased with the increasing power of the laser beam and with the RF modulator was applied it was of 1.06 ppm.

The OBD setup was characterised by the use of the reference EmagCan microstructure with the length, width, and thickness of 450 µm, 60 µm, and 3 µm, respectively. The stiffness of the reference structure was determined through analysis of thermomechanical noise. The noise was recorded using an HeNe interferometer. Calculations were based on the equipartition theorem [28–31]. The thermal deflection amplitude was 4 pm which corresponds to the stiffness

Metrol. Meas. Syst., Vol. 28 (2021), No. 4, pp. 627–642
DOI: 10.24425/mms.2021.137698

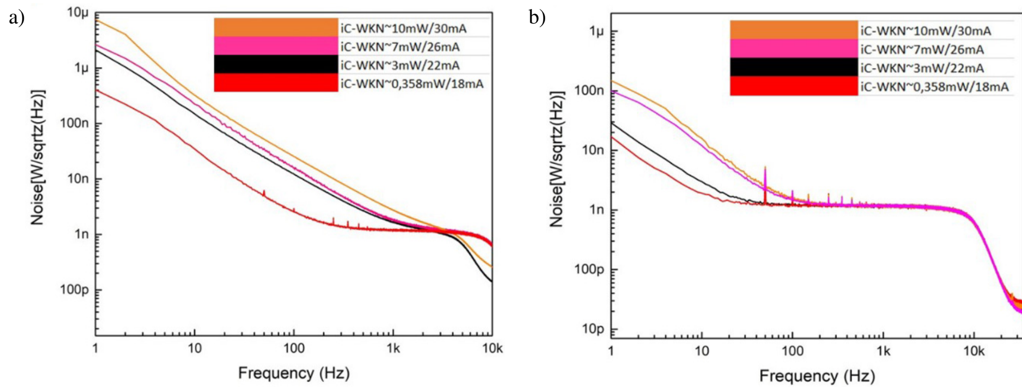

Fig. 7. Low-frequency noise measurement for variable power of the EmagCan OBD laser: a) biased without the RF modulator; b) biased with the RF modulator.

Table 1. Power of the low-frequency noise of the EmagCan OBD laser.

Biased with a RF modulator			**Biased without a RF modulator**		
P [mW]	**Power of the noise (PN) [W]**	**PN/P [ppm]**	**P [mW]**	**Power of noise (PN) [W]**	**PN/P [ppm]**
0.358	1.00E–05	0.28	0.358	1.17E–05	0.33
3	1.01E–05	3.37	3	1.63E–05	5.44
7	1.04E–05	1.49	7	2.38E–05	3.41
10	1.06E–05	1.06	10	3.41E–05	3.41

of 1.02 ± 0.05 N/m in air (Fig. 8a). Analogous measurements and calculations were performed with the OBS setup. Comparison of values from both sources provides information sufficient to characterise an OBD setup.

The investigations were performed for the first and second eigenmode of the EmagCan reference microstructure for six different configurations of the optical setup of the EmagCan OBD system. The detailed parameters of system configuration and the recorded spectra are presented in Fig. 8b and 8c.

In the performed experiments we noticed increased amplitude of the EmagCan reference thermomechanical noise signal following the relationship resulting from the modification of the optical path according to (7). Exchanging the collimator of 6,2 mm focus for one of 4.5 mm focus resulted in an increase in the recorded signal almost equal to the ratio of the focal lengths $6.2/4.5 = 1.4$. This phenomenon was also confirmed when the output signals were calculated for the first and second eigenmode cantilever vibrations. The exchange of the focus lens lead to a similar effect. The ratio of focal lengths of $75/50 = 1.5$ corresponds to the ratio of the recorded signals 30.3 μV/20.7 μV = 1.5. As a result of changing both the collimator lens and the focus lens we noticed amplification of the reference thermal noise according to the relations arising from the product of parameters of components in the optical path. This relation can be described as $(75/50) \times (6.24/4.51) = 2.07$, which is also reflected by the ratio of the thermal signals: 42.1 μV/20.7 μV = 2.04.

We also noticed, that the reference thermal noise was three and half times higher in comparison with the basic EmagCan-OBD setup (configuration 1) when the slit aperture was installed. Fig. 9

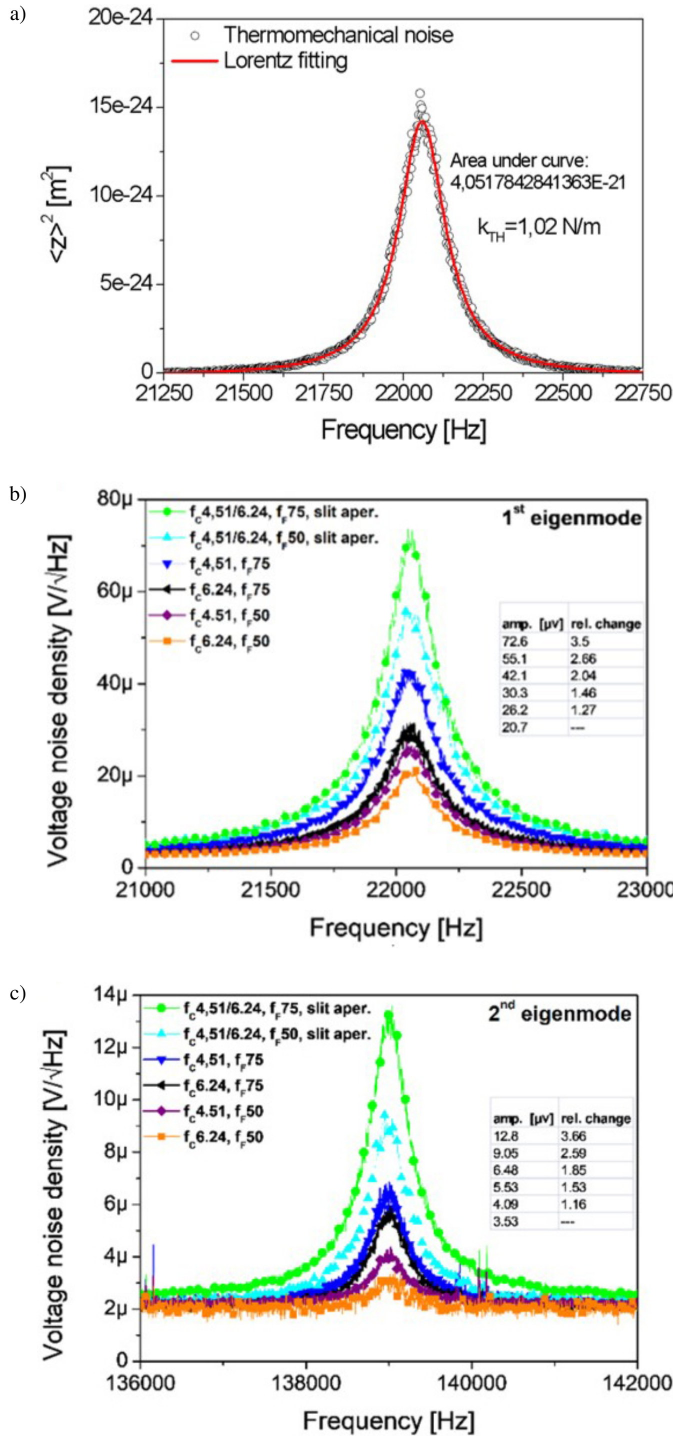

Fig. 8. Thermal noise spectra of the reference EmagCan cantilever: a) registered by a HeNe interferometer; b) first eigenmode; c) second eigenmode.

Metrol. Meas. Syst., Vol. 28 (2021), No. 4, pp. 627–642
DOI: 10.24425/mms.2021.137698

depicts theoretical and experimental laser power dependence of effective deflection noise density n_{zsN} for different widths of the beam. The theoretical values in each case were calculated using (12).

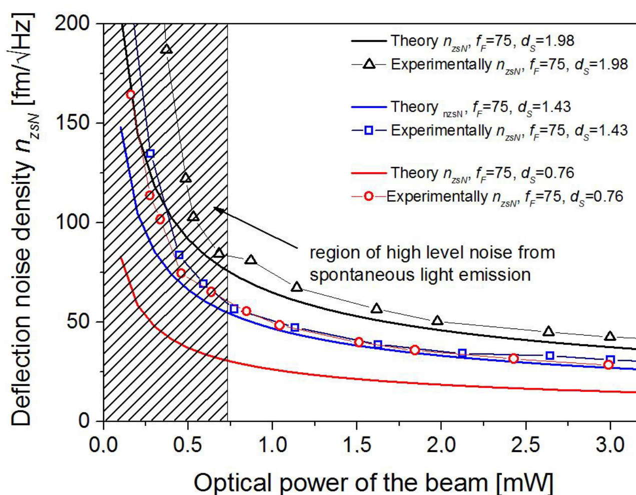

Fig. 9. Theoretical and experimental effective deflection noise density as a function of optical power and width of slit aperture in the optical path. In the performed experiments the reference EmagCan cantilever was used (parameters used in calculations: l = 450 µm, f_F = 75 mm, η = 0.42, α = 0.4) and laser with APC feedback and an RF modulated current.

The analysis of the experimental data shows that for the optical power below 750 µW the total noise of deflection detection was increased. This resulted from the spontaneous light emission of the laser and/or instability in the feedback loop of the APC circuit. As expected, the effective deflection noise density was reduced when the laser power was increased. The decrease in the width of the laser beam resulted in a decrease in the deflection noise, as described in (12). In the case of the beam width of 2.0 mm and 1.4 mm the experimentally measured data agrees well with the theoretical values of the effective deflection noise density – Fig. 9. When the slit aperture was used, the experimental and measured data were not consistent, which was due to the limit introduced by the cantilever thermal noise vibration. As noted in [28,32] the thermal noise depends on the cantilevers resonance frequency, quality factor and stiffness. The calculated thermal noise for the EmagCan reference cantilever was approximately 32 fm/√Hz at the frequency of 10 kHz. The measured deflection noise density of the EmagCan setup was approximately 34 fm/√Hz for the optical power of 3 mW used for the detection. In the case of the cantilevers, whose stiffness was ten times bigger than the stiffness of the reference beam but of the same length, it was expected that the resolution limit was only set by the photodetector shot noise.

The introduced modifications improved also the SNR of the measurement process defined as the ratio between the amplitude of the reference cantilever thermomechanical noise and the thermal noise floor. The measured SNR was higher when the slit aperture was used.

For each thermomechanical spectrum showed in Fig. 8a we calculated the area under the first resonance as the power spectrum obtained from the deflection output signals, scaled into the frequency domain. The area under the curve correlates with mean-square cantilever deflection. Next, we correlated this value with the spring constant of the reference cantilever and thermal energy given by $k_B T$. Finally, the EmagCan-OBD deflection sensitivity obtained from equipartition

theorem takes the form of:

$$S_{V\text{meas}} = \sqrt{k\frac{A}{k_B T}}, \tag{13}$$

where: $S_{V\text{meas}}$ is the experimentally measured sensitivity estimated from thermal noise, k is the previously calibrated reference cantilever stiffness, k_B is the Boltzmann constant, T is the temperature, A is the area under the first resonance peak. The relative change of the sensitivity of the EmagCan-OBD was calculated for each case, and the results are summarized in Table 2.

Table 2. Theoretical and measured value of OBD sensitivity. The calculations were done using (13). The cantilever's nominal length was 450 μm, spring constant 1.02 ± 0.05 N/m, the width of laser spot 2 mm, 1.4 mm, 0.8 mm respectively for the collimation lens of focal lengths 6.2, 4.5 and slit aperture.

No.	f_C [mm]	f_F [mm]	*sa* [–]	*A* [V^2]	$S_{V\text{calc}}$ [mV/nm]	R_{calc} [–]	$S_{V\text{meas}}$ [mV/nm]	S_{meas} [–]
1	6.24	50	no	1,13E–7	5.12	–	5.28	–
2	4.51	50	no	1.37E–7	6.83	1.33	5.83	1.27
3	6.24	75	no	2.46E–7	7.75	1.51	7.78	1.46
4	4.51	75	no	5.05E–7	9.52	2.01	11.16	2.04
5	6.24/4.51	50	yes	8.74E–7	13.7	2.67	14.67	2.66
6	6.24/4.51	75	yes	1.31E-6	17.54	3.42	17.9	3.5

Abbreviations: *sa* – slit aperture, *A* – area under the curve, $S_{V\text{calc}}$ – theoretically calculated sensitivity, $S_{V\text{meas}}$ – experimentally calculated sensitivity from thermal noise, R_{calc} – relative change of the sensitivity for theoretical calculation, R_{meas} – relative change of the sensitivity for experimental calculation.

The calculated and measured sensitivities were in agreement within the margin of 17% in the worst case and 2% for the highest sensitivity obtained in the setup configuration 6 (combining the long focusing lens and the aperture slit). Finally, we obtained resolution of the measurement improved 3.5 times in comparison with the basic EmagCan OBD configuration.

5. Static deflection measurements of EmagCan structures

The constructed and optimized EmagCan-OBD setup was used to calibrate actuation coefficients of the electromagnetically actuated cantilever [22]. The deflection measurement sensitivity and the effective deflection noise density corresponding to cantilever length were calculated using (7) and (12) as equal to 15.3 mV/nm, and 38 fm/$\sqrt{\text{Hz}}$ for 3 mW optical power after the aperture, respectively.

Static deflection of the EmagCan cantilever was investigated when the cantilever was immersed in a static magnetic field and when the current flowing through the loop was biased. This was done by measuring cantilever deflection in response to the step function signal modulating the current in the loop.

The linear electromagnetic cantilever actuation was associated with parasitic thermal actuation which had a quadratic characteristic – Fig. 10b. The parasitic thermal effect stemmed from the Joule heat generated by the current flowing through the loop and from the mismatch of the thermal expansion coefficients for silicon and gold. Both phenomena led to biomorphic behaviour of the cantilever beam. The actuation coefficients of the calibrated Emag cantilever were 19.51 nm/mA for the electromagnetic component, and 9.21 nm/mA^2 for the thermal component, as can be derived from performed measurements.

Metrol. Meas. Syst., Vol. 28 (2021), No. 4, pp. 627–642
DOI: 10.24425/mms.2021.137698

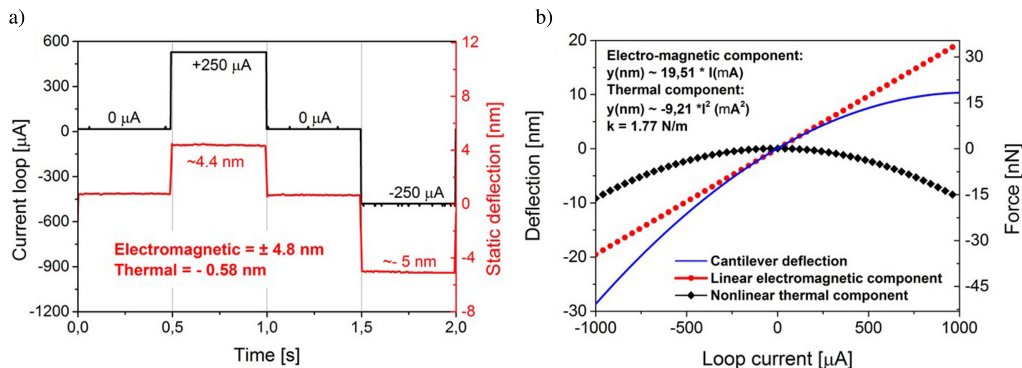

Fig. 10. a) Cantilever static deflection in response to a step function signal; b) Pseudo-static (low frequency) actuation characteristics of a 1.77 N/m microcantilever measured in 0.48 T magnetic field with thermal and magnetic actuation components extracted.

6. Conclusions

Theoretical analysis and experimental verification of the EmagCan-OBD method for metrology of the electromagnetic cantilevers were presented. Analytical formulas allowing the assessment of the performance improvements of the deflection sensitivity and SNR were given. The proposed optimization method provided significant improvement in the deflection sensitivity and SNR without a need for significant changes in the measurement head. Both analytic and experimental studies showed that optical OBD measurement sensitivity increased with a decrease in the width of the optical spot. The optimized and calibrated setup was used to characterize an electromagnetically actuated cantilever. We also demonstrated precise, bidirectional control of cantilever apex position and/or force exerted on it. The proposed technology is vital for future applications in which the precise and bidirectional actuation of the probe cantilever is needed. Moreover, basing on this metrology technique it will be possible to optimize the manufacturing of future electromagnetic cantilevers. In this case the influence of thermomechanical actuation, as the one which is more difficult to be controlled, should be reduced. The application of the high resolution measurement methods making it possible to characterize the static cantilever deflection is of great importance and the proposed methodology is one of the needed solutions.

Acknowledgements

This work was supported by the National Science Centre, Poland OPUS grant "Nanometrology of Nottingham cooling effect using operational microelectromechanical systems" (project No. 2020/37/B/ST7/03792).

References

[1] Binnig, G., Quate, C. F., & Gerber, C. (1986). Atomic force microscope. *Physical Review Letters*, *56*(9), 930. https://doi.org/10.1103/PhysRevLett.56.930

[2] Judy, J. W. (2001). Microelectromechanical systems (MEMS): fabrication, design and applications. *Smart Materials and Structures*, *10*(6), 1115–1134. https://doi.org/10.1088/0964-1726/10/6/301

[3] Algamili, A. S., Khir, M. H. M., Dennis, J. O., Ahmed, A. Y., Alabsi, S. S., Hashwan, S. S. B., & Junaid, M. M. (2021). A review of actuation and sensing mechanisms in MEMS-based sensor devices. *Nanoscale Research Letters*, *16*(1), 1–21. https://doi.org/10.1186/s11671-021-03481-7

[4] Woszczyna, M., Gotszalk, T., Zawierucha, P., Zielony, M., Ivanow, Tzv., Ivanowa, K., Sarov, Y., Nikolov, N., Mielczarski, J., Mielczarska, E., & Rangelow, I. W. (2009). Thermally driven piezoresistive cantilevers for shear-force microscopy. *Microelectronic Engineering*, *86*(4), 1212–1215. https://doi.org/10.1016/j.mee.2009.01.043

[5] Shen, B., Allegretto, W., Hu, M., & Robinson, A. M. (1996). CMOS micromachined cantilever-in-cantilever devices with magnetic actuation. *IEEE Electron Device Letters*, *17*(7), 372–374. https://doi.org/10.1109/55.506371

[6] Adhikari, R., Kaundal, R., Sarkar, A., Rana, P., & Das, A. K. (2012). The cantilever beam magnetometer: A simple teaching tool for magnetic characterization. *American Journal of Physics*, *80*(3), 225–231. https://doi.org/10.1119/1.3679840

[7] Hsieh, C. H., Dai, C. L., & Yang, M. Z. (2013). Fabrication and Characterization of CMOS-MEMS Magnetic Microsensors. *Sensors*, *13*(11), 14728–14739. https://doi.org/10.3390/s131114728

[8] Rhoads, J. F., Kumar, V., Shaw, S. W., & Turner, K. L. (2013). The non-linear dynamics of electromagnetically actuated microbeam resonators with purely parametric excitations. *International Journal of Non-Linear Mechanics*, 55, 79–89. https://doi.org/10.1016/j.ijnonlinmec.2013.04.003

[9] Lee, B., Prater, C. B., & King, W. P. (2012). Lorentz force actuation of a heated atomic force microscope cantilever. *Nanotechnology*, *23*(5), 055709. https://doi.org/10.1088/0957-4484/23/5/055709

[10] Neuman, K. C., & Nagy, A. (2008). Single-molecule force spectroscopy: optical tweezers, magnetic tweezers and atomic force microscopy. *Nature Methods*, *5*(6), 491–505. https://doi.org/10.1038/nmeth.1218

[11] Hoogenboom, B. W., Frederix, P. L. T. M., Yang, J. L., Martin, S., Pellmont, Y., Steinacher, M., Zäch, S., Langenbach, E., Heimbeck, H.-J., Engel, A., & Hug, H. J. (2005). A Fabry–Perot interferometer for micrometer-sized cantilevers. *Applied Physics Letters*, *86*(7), 074101-1. https://doi.org/10.1063/1.1866229

[12] Meyer, G., & Amer, N. M. (1988). Novel optical approach to atomic force microscopy. *Applied Physics Letters*, *53*(12), 1045–1047. https://doi.org/10.1063/1.100061

[13] Boisen, A., Dohn, S., Keller, S. S., Schmid, S., & Tenje, M. (2011). Cantilever-like micromechanical sensors. *Reports on Progress in Physics*, *74*(3), 036101. https://doi.org/10.1088/0034-4885/74/3/036101

[14] Gimzewski, J. K., Gerber, Ch., Meyer, E., & Schlittler, R. R. (1994). Observation of a chemical reaction using a micromechanical sensor. *Chemical Physics Letters*, *217*(5), 589–594. https://doi.org/10.1016/0009-2614(93)E1419-H

[15] Wu, G., Ji, H., Hansen, K., Thundat, T., Datar, R., Cote, R., Hagan, M. F., Chakraborty, A. K., & Majumdar, A. (2001). Origin of nanomechanical cantilever motion generated from biomolecular interactions. *Proceedings of the National Academy of Sciences*, *98*(4), 1560–1564. https://doi.org/10.1073/pnas.98.4.1560

[16] Nieradka, K., Kapczyńska, K., Rybka, J., Lipiński, T., Grabiec, P., Skowicki, M., & Gotszalk, T. (2014). Microcantilever array biosensors for detection and recognition of Gram-negative bacterial endotoxins. *Sensors and Actuators B: Chemical*, *198*, 114–124. https://doi.org/10.1016/j.snb.2014.03.023

[17] Helm, M., Servant, J. J., Saurenbach, F., & Berger, R. (2005). Read-out of micromechanical cantilever sensors by phase shifting interferometry. *Applied Physics Letters*, *87*(6), 064101. https://doi.org/10.1063/1.2008358

Metrol. Meas. Syst., Vol. 28 (2021), No. 4, pp. 627–642
DOI: 10.24425/mms.2021.137698

[18] Putman, C. A. J., de Grooth, B. G., van Hulst, N. F., & Greve, J. (1992). A theoretical comparison between interferometric and optical beam deflection technique for the measurement of cantilever displacement in AFM. *Ultramicroscopy*, *42*, 1509–1513. https://doi.org/10.1016/0304-3991(92)90474-X

[19] Putman, C. A. J., de Grooth, B. G., van Hulst, N. F., & Greve, J. (1992). A detailed analysis of the optical beam deflection technique for use in atomic force microscopy. *Journal of Applied Physics*, *72*(1), 6–12. https://doi.org/10.1063/1.352149

[20] Hu, Z., Seeley, T., Kossek, S., & Thundat, T. (2004). Calibration of optical cantilever deflection readers. *Review of Scientific Instruments*, *75*(2), 400–404. https://doi.org/10.1063/1.1637457

[21] Fukuma, T., Kimura, M., Kobayashi, K., Matsushige, K., & Yamada, H. (2005). Development of low noise cantilever deflection sensor for multienvironment frequency-modulation atomic force microscopy. *Review of Scientific Instruments*, *76*(5), 053704. https://doi.org/10.1063/1.1896938

[22] Nieradka, K., Kopiec, D., Małozięć, G., Kowalska, Z., Grabiec, P., Janus, P., Sierakowski, A., Domański, K., & Gotszalk, T. (2012). Fabrication and characterization of electromagnetically actuated microcantilevers for biochemical sensing, parallel AFM and nanomanipulation. *Microelectronic Engineering*, *98*, 676–679. https://doi.org/10.1016/j.mee.2012.06.019

[23] Miyatani, T., & Fujihira, M. (1997). Calibration of surface stress measurements with atomic force microscopy. *Journal of Applied Physics*, *81*(11), 7099–7115. https://doi.org/10.1063/1.365306

[24] Mishra, R., Grange, W., & Hegner, M. (2012). Rapid and reliable calibration of laser beam deflection system for microcantilever-based sensor setups. *Journal of Sensors*, *2021*, 617386. https://doi.org/10.1155/2012/617386

[25] Naeem, S., Liu, Y., Nie, H. Y., Lau, W. M., & Yang, J. (2008). Revisiting atomic force microscopy force spectroscopy sensitivity for single molecule studies. *Journal of Applied Physics*, *104*(11), 114504. https://doi.org/10.1063/1.3037206

[26] Lee, J., Beechem, T., Wright, T. L., Nelson, B. A., Graham, S., & King, W. P. (2006). Electrical, thermal, and mechanical characterization of silicon microcantilever heaters. *Journal of Microelectromechanical Systems*, *15*(6), 1644–1655. https://doi.org/10.1109/JMEMS.2006.886020

[27] Skwierczyński, J. M., Małozięć, G., Kopiec, D., Nieradka, K., Radojewski, J., & Gotszalk, T. (2011). Radio frequency modulation of semiconductor laser as an improvement method of noise performance of scanning probe microscopy position sensitive detectors. *Optica Applicata*, *41*(2), 323–331.

[28] Butt, H.-J., & Jaschke, M. (1995). Calculation of thermal noise in atomic force microscopy. *Nanotechnology*, *6*(1), 1. https://doi.org/10.1088/0957-4484/6/1/001

[29] Ohler, B. (2007). Cantilever spring constant calibration using laser Doppler vibrometry. *Review of Scientific Instruments*, *78*(6), 063701. https://doi.org/10.1063/1.2743272

[30] Cleveland, J. P., Manne, S., Bocek, D., & Hansma, P. K. (1993). A nondestructive method for determining the spring constant of cantilevers for scanning force microscopy. *Review of Scientific Instruments*, *64*(2), 403–405. https://doi.org/10.1063/1.1144209

[31] Lévy, R., & Maaloum, M. (2002). Measuring the spring constant of atomic force microscope cantilevers: thermal fluctuations and other methods. *Nanotechnology*, *13*(1), 33. https://doi.org/10.1088/0957-4484/13/1/307

[32] Rast, S., Wattinger, C., Gysin, U., & Meyer, E. (2000). The noise of cantilevers. *Nanotechnology*, *11*(3), 169. https://doi.org/10.1088/0957-4484/11/3/306

Daniel Kopiec received the MSc degree from Faculty of Microsystem Electronics and Photonics of Wrocław University of Technology in 1999. His scientific interests are: design of analog and digital electronic circuits for micro- and nanomechanical devices. Currently, he is pursuing his PhD degree at Wrocław University of Technology, focusing on application of electromagnetically actuated cantilever in SPM technique and sensor application.

Wojciech Majstrzyk received the MSc degree from Faculty of Microsystem Electronics and Photonics, Wrocław University of Technology in 2013. Currently, he is pursuing his PhD degree at Wrocław University of Technology, focusing on application of cantilevers array for force and mass measurements.

Dominik Badura received the B.Sc. degree in Nanotechnology and Technologies of Material Processes from Silesian University of Technology in Gliwice in 2019 and M.Sc. degree in Electronic and Telecommunication from Wrocław University of Science and Technology in 2020. Currently, he is pursuing his PhD at the Doctoral School of Wrocław University of Science and Technology in the field of Automation, Electronic and Electrical Engineering. He focuses on nanometrology and fast microscopy of AFM micro- and nanostructures.

Bartosz Pruchnik he received the MSc degree from Faculty of Mechanical Engineering, Wrocław University of Science and Technology in 2020. Currently, he is pursuing his PhD degree at Wrocław University of Science and Technology, focusing on mechanoenergetic aspects of micromechanical devices and measurements.

Ewelina Gacka received the B.Sc. degree in Technical Physics in 2018 and the M.Sc. degree in Optoelectronics and Telecommunication in 2019, both from Wrocław University of Science and Technology. Currently, she is pursuing her PhD at the Doctoral School of Wrocław University of Science and Technology in the field of Automation, Electronic and Electrical Engineering. She focuses on nanometrology and fabrication of MEMS/NEMS devices with the focused electron beam.

Andrzej Sierakowski received the M.Sc. degree from the Faculty of Mechatronics, Warsaw University of Technology in 2001. He is a technical engineering senior specialist at the Division of Silicon Microsystems and Nanostructure Technology, Institute of Electron Technology (ITE), in Warsaw. He is responsible for photolithography processing, masks designing and fabrication in semiconductor technology and MEMS/MOEMS devices based on silicon micromachining and other applications requiring high pattern precision and resolution. His research presently focuses on developing an atomic force microscopy measurements for photolithography application.

Pawel Janus received the B.Sc. and M.Sc. degrees from the Technical University in Wrocław, Poland in 1996 and 1998, respectively. In 2003 he received the PhD degree in Electrical Engineering from the Faculty of Microsystems Electronics and Photonics, Wrocław University of Technology, Poland. Since 2003 he has been with the Institute of Electron Technology (ITE), Warsaw. His research interests include studies of materials for MEMS applications, micromachining of silicon microstructures, microsensors, and microactuators. His current research is silicon force sensor development for nano-mechanical applications. He is the author and co-author of more than 50 technical papers presented in journals and at conferences.

Teodor Paweł Gotszalk received the MSc degrees from the Faculties of Electronics and of Electrical Engineering of Wrocław University of Technology in 1989 and 1991, respectively. In 1996, he received the PhD degree from the Institute of Electronic Technology, Wrocław University of Technology. He has been honored for his scientific work with the Siemens Research Award in 2000 and the prize of the Polish Science Foundation (FNP) in 1997. He is Head of the Division of Micro- and Nanostructures Metrology at the Faculty of Microsystems Electronics and Photonics of Wrocław University of Technology. He has authored over 100 scientific publications.